JOURNAL OF SPACECRAFT AND ROCKETS
Vol. 41, No. 3, May–June 2004

Fuzzy Logic Trajectory Design and Guidance for Terminal Area Energy Management

Bradley T. Burchett*
Rose–Hulman Institute of Technology, Terre Haute, Indiana 47803

The second-generation reusable launch vehicle will incorporate sophisticated new guidance and control methods to increase the system's flexibility, in particular making it a practical vehicle for unmanned cargo missions. This project focuses on trajectory design and guidance for the terminal area energy management phase of flight, where traditional methods have produced limited results. Fuzzy logic methods are used to make onboard autonomous gliding return trajectory design robust to the possibility of control surface failures, thus, increasing the flexibility of unmanned gliding recovery and landing. Fuzzy inference systems are used to design the trajectory and provide guidance commands for the vehicle bank angle and negative z axis acceleration. Fuzzy logic provides a practical means of incorporating conflicting objectives and constraints in choosing trajectory parameters. The method has the flexibility to choose these parameters from a continuum of possible values. The design is validated using a high-fidelity six-degree-of-freedom simulation of the X-33 technology demonstrator.

Nomenclature

C_D = drag coefficient
c_2 = dimensionless coefficient used to determine h_{ref}
c_3 = coefficient used to determine h_{ref}, ft^{-1}
c_4 = coefficient used to determine h_{ref}, ft^{-2}
D = drag force, lbf
E_{MEP} = energy over weight for minimum entry point (MEP) approach
E_N = energy over weight for nominal approach
E_W = vehicle energy divided by weight, ft
g = gravity constant, 32.174 ft/s^2
h = vehicle c.g. height above runway, ft
h_{ref} = reference altitude, ft
m = vehicle mass, slug
N_Z = vehicle negative z axis component of acceleration, g
r_H = vehicle turn radius in the horizontal plane, ft
r_{HAC} = radius of heading alignment turn, ft
r_V = vehicle turn radius in the vertical plane, ft
S = vehicle frontal area, ft^2
SL = energy over weight for large s-turn approach
SM = energy over weight for medium s-turn approach
SS = energy over weight for small s-turn approach
V = forward velocity, ft/s
V_{HAC} = expected velocity at heading alignment cone (HAC) initiation, ft/s
X_{ALI} = X runway coordinate of baseline autolanding interface (ALI) point
X_{FTC} = nominal value for X_{HAC}
X_{HAC} = X runway coordinate of HAC center
X_{MAX} = X_{HAC} value for maximum energy approach
X_{MEP} = X runway coordinate for MEP approach
x = vehicle c.g. distance from runway threshold, ft
y = vehicle c.g. distance from runway centerline, ft
γ = flight-path angle, deg
ρ = atmospheric density, slug/ft^3
ϕ = bank angle, deg
$\phi_{\max}$ = maximum bank angle during HAC turn, deg
ψ = heading angle with respect to runway, deg

Received 5 November 2002; revision received 18 July 2003; accepted for publication 18 July 2003.

*Assistant Professor, Department of Mechanical Engineering. Senior Member AIAA.

Introduction

THE second-generation reusable launch vehicle will leverage many new technologies to make flight to low Earth orbit safer and more cost effective. One important capability will be completely autonomous flight during reentry and landing, thus, making it unnecessary to crew the vehicle for cargo missions with stringent weight constraints. Implementation of sophisticated new guidance and control methods will enable the vehicle to return to Earth under less than favorable conditions.

The return to Earth consists of three phases: entry, terminal area energy management (TAEM), and approach and landing (A/L). Entry is defined as taking the spacecraft from entry interface to 90,000 ft above mean sea level. TAEM takes the spacecraft from 90,000 ft above mean sea level and Mach 3 to 10,000 ft and Mach 0.5 and aligns the craft with the extended runway centerline. A/L takes the vehicle from 10,000 ft to wheel stop on the runway. The Space Shuttle is programmed to fly all three phases of flight automatically, and under normal circumstances the astronaut-pilot takes manual control only during the A/L phase. The automatic control algorithms used in the shuttle for TAEM and A/L have been developed over the past 30 years. They are computationally efficient and based on careful study of the spacecraft's flight dynamics, and heuristic reasoning. During flight, the existing guidance may adjust certain trajectory parameters by choosing from a few discrete values.

With the advent of the X-33 and X-34 technology demonstration vehicles, several authors investigated implementing advanced control methods to provide autonomous real-time design of gliding return trajectories, thus enhancing the ability of the vehicle to adjust to widely dispersed energy states.[1–4] The bulk of work published to date deals primarily with the approach and landing phase of flight. In Ref. 1, the focus is on the autolanding trajectory, where changes in heading angle are small and the distance to runway threshold is monotonically decreasing. In Ref. 2, new methods are proposed to assess the robustness of autolanding trajectories. In Ref. 3 results are shown for the subsonic portion of TAEM. In Ref. 4, an adaptive-critic neural network approach is used to optimize trajectory design for the A/L phase of flight. Once again, the mathematics used are only applicable when the heading changes are small and the distance to the runway is monotonically decreasing.

Of the four references mentioned, only in Ref. 1 are results presented for TAEM and then only for the subsonic portion. Thus, the author is led to believe that little or no work has been published introducing novel methods for designing and flying the return trajectory

including the supersonic portion of TAEM. In this project, fuzzy logic methods are used to design gliding autonomously return trajectories from the entry guidance interface to autolanding interface (ALI). Existing shuttle TAEM in-flight trajectory adjustments are facilitated by a series of crisp logic decisions. For instance, the length of final approach can be selected from three discrete values based on energy dispersion. In contrast to existing methods, fuzzy logic methods choose from a continuum of possible values for trajectory parameters. Because the energy state varies gradually, trajectory parameters will be adjusted gradually so that the planned trajectory could potentially provide the best possible energy profile at each guidance cycle. Fuzzy logic provides a straightforward way to balance multiple constraints and objectives in a single decision. Also, fuzzy logic tends to be very robust to plant model uncertainty. This is particulary advantageous in the sequel, where the guidance system is developed based on an approximate plant model, but performs rather well after integrating with a much more realistic model.

The system described here is intended to be part of a larger advanced guidance and control structure. Hanson[5] provides one possible architecture for the overall system. This work describes a novel approach to trajectory generation and closed-loop guidance only. Control surface failures would be detected during entry or TAEM phase by the system identification subsystem, which is being developed by others. In particular, the fuzzy logic method provides the capability of compensating for control surface failures by restricting the allowable bank angle used during the trajectory. Results of a high-fidelity simulation are presented for the entire TAEM phase from Mach 3 and 90,000 ft to ALI at approximately Mach 0.5 and 10,000 ft. The method provides a flyable trajectory with bank restricted to 36 deg, thus, increasing the flexibility of unmanned gliding recovery and landing.

Simplified Model of Gliding Vehicle Dynamics

The following equations, provided by Vinh,[6] describe the motion of an aircraft flying over a flat, nonrotating Earth:

$$\dot{V} = \frac{1}{m}F_T - g\sin\gamma \tag{1}$$

$$V\dot{\gamma} = \frac{1}{m}F_N\cos\phi - g\cos\gamma \tag{2}$$

$$V\dot{\psi} = \frac{F_N\sin\phi}{m\cos\gamma} \tag{3}$$

where we have used ϕ to denote aircraft bank angle. F_N and F_T are the aerodynamic force components normal and tangential to the velocity vector, respectively. Assuming that angle of attack α and sideslip angle β are small, we can equate F_N with lift and F_T with drag, that is, $F_T = -D$ and $F_N = L$. To decouple Eqs. (2) and (3), also assume that $\dot{\gamma} = \gamma \cong 0$. This reduces Eq. (2) to

$$L\cos\phi - mg = 0 \tag{4}$$

which can be solved for lift L, yielding

$$L = mg/\cos\phi \tag{5}$$

Substitute the kinematic relationship for curvilinear motion $\dot{\psi} = V/r_H$, where r_H is the instantaneous turn radius in the horizontal plane; then Eq. (3) reduces to

$$L\sin\phi = m(V^2/r_H) \tag{6}$$

Equation (5) is then substituted for lift in Eq. (6), resulting in an expression for instantaneous horizontal turn radius that is independent of aircraft size or type:

$$r_H = (V^2/g)(1/\tan\phi) \tag{7}$$

Now substituting $\dot{\psi}^2 r_H = V^2/r_H$ in Eq. (7) and solving for turn rate $\dot{\psi}$ results in the following:

$$\dot{\psi} = (g/V)\tan\phi \tag{8}$$

To find the corresponding decoupled flight-path angle equation, assume zero bank angle in Eq. (2):

$$\dot{\gamma} = (1/V)(L/m - g\cos\gamma) \tag{9}$$

With substitution of the kinematic relation for curvilinear motion in the vertical plane $\dot{\gamma} = V/r_V$ and rearrangement, the following three quantities are equal:

$$L - mg\cos\gamma = m(V^2/r_V) = N_Z m \tag{10}$$

Solving for instantaneous turn radius in the vertical plane yields

$$r_V = \frac{mV^2}{L - mg\cos\gamma} \tag{11}$$

Solving Eq. (10) for negative z axis acceleration N_Z renders

$$N_Z = L/m - g\cos\gamma \tag{12}$$

Finally, substituting Eq. (12) into Eq. (9) will eliminate lift and, thus, make the model independent of specific aircraft aerodynamic properties,

$$\dot{\gamma} = N_Z/V \tag{13}$$

Equation (1) is rewritten in terms of drag:

$$\dot{V} = -D/m - g\sin\gamma \tag{14}$$

where drag D is given by

$$D = \tfrac{1}{2}\rho V^2 S C_D \tag{15}$$

By definition of heading angle ψ and flight-path angle γ, the aircraft position in x–y–h space is governed by the following equations:

$$\dot{x} = V\cos\gamma\cos\psi \tag{16}$$

$$\dot{y} = V\cos\gamma\sin\psi \tag{17}$$

$$\dot{h} = V\sin\gamma \tag{18}$$

Atmospheric density is determined from the exponential model[7]

$$\rho = \begin{cases} 0.0023784722(1 - 6.8789\times10^{-6}h)^{4.258}, & h < 35{,}332 \\ 0.00072674385\exp[-4.78\times10^{-5}(h - 35332)], & h \geq 35{,}332 \end{cases} \tag{19}$$

Equations (8), (13), (14), and (16–18) provide a generic aerospace vehicle model where only the drag coefficient is aircraft specific. The coefficient of drag was taken to be a function of Mach number only and was approximated by the zero lift portion of the drag table directly from a high-fidelity nonlinear simulation of the X-33 vehicle. These drag coefficient data are shown in Fig. 1. Induced drag was ignored, which is probably the biggest weakness in the simplified model. The resulting model was programmed in MATLAB®/Simulink to serve as a testbed for rapid prototyping,

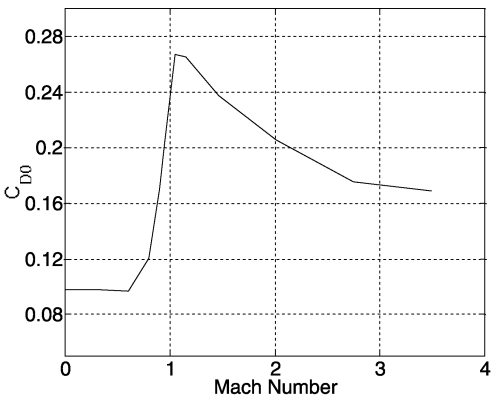

Fig. 1 Simplified model drag coefficient.

tuning, and testing of fuzzy inference systems for trajectory design and guidance.

When Eqs. (8), (13), (14), and (16–18) are examined, it should be clear that vehicle ground track is controlled primarily by bank angle ϕ, the altitude is controlled by normal acceleration N_Z, and the dynamic pressure $\bar{q} = 1/2\rho V^2$ is controlled by either changing the flight-path angle γ, or by changing the coefficient of drag C_D (by extending drag devices).

The simplified dynamics were simulated in the MATLAB/Simulink environment and used for extensive trial-and-error design of the fuzzy logic trajectory design and guidance algorithm. Although these dynamics appear overly simplified, they provided an adequate testbed for development of the fuzzy rules. Flight-path angle magnitude for an actual gliding return trajectory does not exceed 30 deg and remains below 26 deg for half of the trajectory. Thus, ignoring the pitch effect on the horizontal flight-path equations has little effect. Also, the inner-loop controller divides the guidance N_Z command by the cosine of current bank angle to compensate for the effect of bank. This justifies ignoring the effect of bank when computing the N_Z command to compensate for altitude. N_Z commands to compensate for altitude are limited to $\pm 0.6\ g$ to avoid exceeding the lift capabilities of the vehicle.

Brief Introduction to Fuzzy Inference Systems

Fuzzy logic and approximate reasoning refer to a method of programming a computer to make decisions in an approximate way, similar to the way humans do. In a sense, it is an extension of crisp logic. In crisp logic, a number either belongs to a set or does not. In fuzzy logic, a number may have partial membership in a set. For example, in crisp logic, the terms hot, comfortable, and cold must have crisp boundaries. Depending on the acclimation of the observer, we might assign boundaries as, for example, if $T < 65°$F, it is cold; if $65 \leq T \leq 80°$F, it is comfortable; and if $T > 80°$F, it is hot. This logic connects the qualitative adjectives hot, comfortable, and cold with specific quantities. However, because the adjectives are intended to be qualitative, and most human reasoning deals with thoughts or ideas rather than numbers, a better numerical representation of the adjectives is sought.

Fuzzy sets allow numbers to have partial membership in a set. Partial membership is determined by the height of the membership function at a particular numerical value. Membership functions can have any shape including triangular, trapezoidal, Gaussian, etc. For example, we might fuzzify the preceding example by assigning the membership functions shown in Fig. 2 to the adjectives used. The range of possible values for a fuzzy input is termed the universe of discourse. The truth value is synonymous with the degree of membership of a particular number.

Now, if the temperature is 68°F, the term cold has a truth value of 0.4, and comfortable has a truth value of 0.6. Assignment of truth values is called fuzzification.

A fuzzy inference system combines fuzzification with a set of if–then rules called the inference engine and an output scheme called defuzzification.[8] Consider the normal acceleration guidance commands inference systems as a somewhat richer example. The input membership functions are shown in Fig. 3. Throughout this work we use the abbreviations P for positive, Z for zero, N for negative, and the adjective prefixes S for small, M for medium, and L for large; for example, LN denotes large negative. Suppose that the current altitude error is 1250 ft, and the current vertical velocity error is 200 ft/s. By examining the input membership functions, we see that $h_{\text{err}} = \text{P}$ and $h_{\text{err}} = \text{Z}$ each have a truth value of 0.5. Vertical velocity error $\dot{h}_{\text{err}} = \text{P}$ has a truth value of 1. The rules for N_Z command are shown in Table 1. The first column is the vertical velocity error and the first row is the altitude error. All of the rules have the following form:

$$\text{If } h_{\text{err}} \text{ is } X \text{ and } \dot{h}_{\text{err}} \text{ is } Y, \text{ then } N_Z \text{ is } Z$$

For instance, in the current illustration, one would enter the P column for altitude error and the P row for vertical velocity error and see that the directed output is LP. This output would be given a weight equal to the minimum degree of membership of the relevant inputs, in this case, 0.5. A second rule is also active because $h_{\text{err}} = \text{Z}$ also has a nonzero degree of membership. The second rule is assessed by entering the Z column and P row of Table 1 and reading N_Z is P from the rule base. This output membership function is also given a truth value of 0.5. The output membership functions for N_Z are shown in Fig. 4b.

Throughout this work, product implication is used. That is, the output membership function is multiplied by the truth value of the relevant rule. When more than one rule is active, maximum value aggregation is used. This is done by searching the universe of discourse of the output variable and assigning an output profile equal at each search point to the maximum of any implicated ouput membership function at that point. The aggregated output universe of discourse for this example is shown in Fig. 5.

Once an aggregated output profile, a fuzzy quantity, is found, we must defuzzify to provide a useful crisp number to the actuators. In this work, centroidal defuzzification is used exclusively. Centroidal or center of gravity defuzzification is performed by treating the output profile as a series of point masses along a line and finding the center of gravity along that line. It can be performed using the

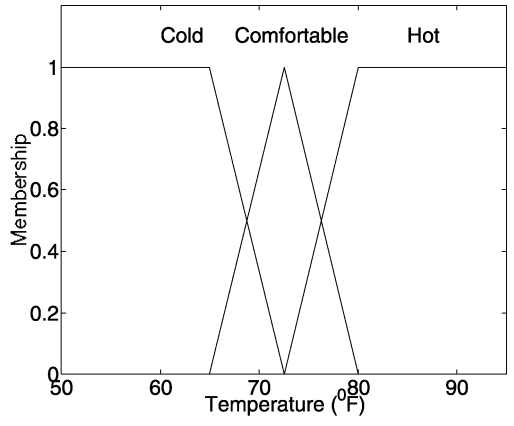

Fig. 2 Membership functions for temperature example.

Table 1 Rules for determining negative *Z*-axis acceleration from inputs altitude error and vertical velocity error

Vertical velocity error	LP	P	Z	N	LN
Z	LP	P	Z	N	LN
LN	Z	N	LN	LN	LN
N	P	Z	N	LN	LN
P	LP	LP	P	Z	N
LP	LP	LP	LP	P	Z

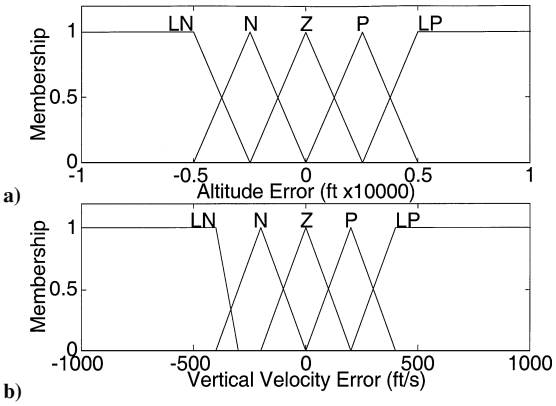

Fig. 3 Partitioning of altitude error and vertical velocity error membership functions.

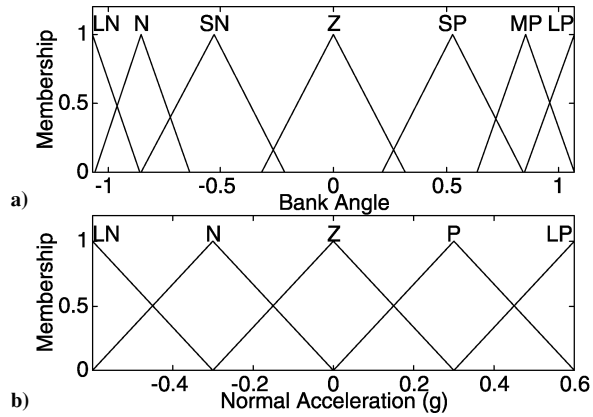

Fig. 4 Partitioning of bank angle and normal acceleration outputs.

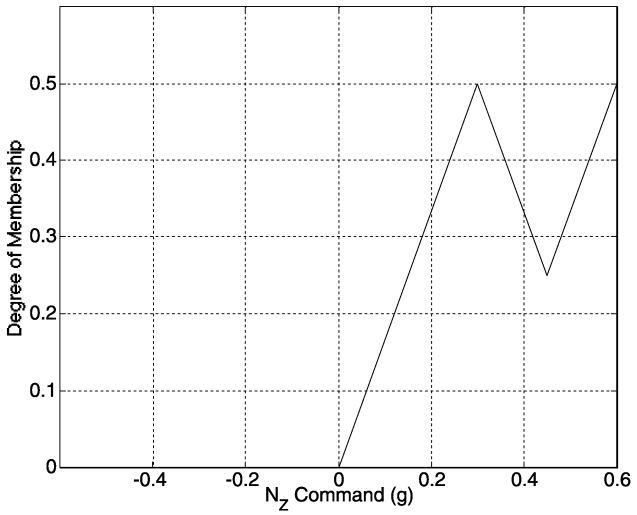

Fig. 5 Aggregate output universe of discourse for N_Z example.

simple geometric average[9]

$$y_c = \frac{\int y\mu_A(y)\,\mathrm{d}y}{\int \mu_A(y)\,\mathrm{d}y} \tag{20}$$

where y is the output variable, μ_A is the aggregate output universe of discourse, a function of y as shown in Fig. 5, and y_c is the resulting crisp output. Typically, defuzzification is actually computed from a discretized aggregate output universe of discourse, such that the integrations are implemented as summations. For the current illustration, the resulting N_Z command is 0.3388 g. Fuzzy logic control has been used in a wide array of applications including approach and landing control of a light aircraft.[10]

Fuzzy Logic Reference Trajectory Design

Given the dynamics of Eqs. (8), (13), (14), and (16–18), and the wealth of knowledge from shuttle heritage, we divided the reference trajectory design into three distinct channels: ground track, altitude, and dynamic pressure. For each channel, we constrained the trajectory to a shape that intentionally limits the number of parameters needed to describe it. Also, a number of acronyms used in this work follow directly from shuttle heritage.

The reference ground path is patterned after a typical tactical air navigation (TACAN) approach flown by military aircraft.[11] The basic geometry is shown in Fig. 6. The spacecraft flies a shortest direction acquisition turn to point directly to the heading alignment cone (HAC) center, a straight portion, and a base to final HAC turn. Turning directly at the HAC center allows a definite transition to HAC phase and provides that the HAC intercept may be flown based on the techniques used by military pilots. Each turn is designed

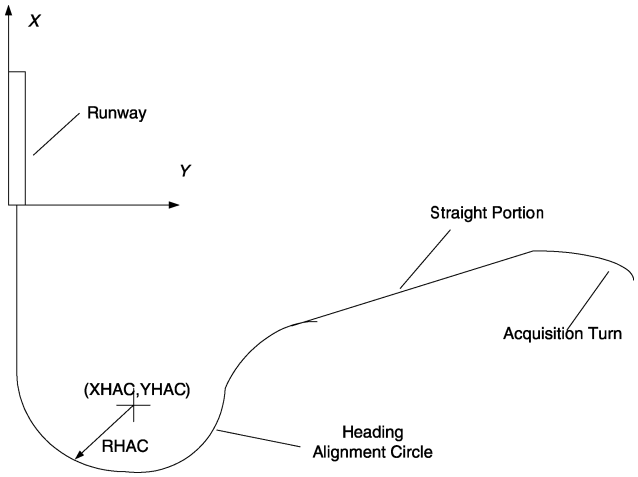

Fig. 6 Baseline trajectory geometry.

as a circular arc. Finally, for each channel, important parameters defining the trajectory are determined through a fuzzy logic decision. The adjustable parameters in the horizontal channel are the heading alignment turn radius Y_{HAC}, and position from the runway threshold X_{HAC}.

The vertical reference trajectory is constrained by initial and final conditions. The spacecraft must reach the ALI at approximately 10,000 ft above the runway, 20,000 ft from the runway threshold at a flight-path angle depressed 30 deg from horizontal. To maintain continuity throughout the trajectory, the vertical path is defined as a cubic polynomial that intersects the ALI at the appropriate altitude and slope,

$$h_{\mathrm{ref}} = c_4 R_{\mathrm{ALI}}^3 + c_3 R_{\mathrm{ALI}}^2 - c_2 R_{\mathrm{ALI}} + h_{\mathrm{ALI}}$$

that is, $c_2 = \mathrm{d}h/\mathrm{d}R = \tan\gamma$, and because $\gamma = -30$ deg at ALI, $c_2 = -0.5774$. Coefficient c_4 is kept constant for simplicity at 1.581×10^{-11} (ft^{-2}). R_{ALI} is the predicted ground track distance to ALI, h_{ALI} is the desired height at ALI, and c_3 is an adjustable parameter allowing real-time updates of the reference vertical path to match off-nominal energy conditions. Coefficient c_3 is allowed to vary between $-1.2(10^{-6})$ and $-3.0(10^{-7})$ (ft^{-1}). The reference vertical velocity is calculated from the time derivative of this cubic. This calculation is provided by the existing guidance and is only modified by adjustments in c_3.

We designed a two-input three-output fuzzy inference system to determine X_{HAC}, Y_{HAC}, and c_3 based on the spacecraft current energy state and control surface health. The inputs are the quotient of energy over predicted downrange distance to ALI E_W/R_{ALI} and an integer denoting the degree of control surface health. Energy is computed as the sum of kinetic and potential energy divided by weight and has dimensions of length:

$$E_W = h + V^2/2g \tag{21}$$

Distance to ALI is computed using the expected ground track from the previous design iteration. The calculations are very similar to those used in shuttle TAEM guidance. All design and guidance operations described are iterated at a rate of 2 Hz. The quotient of energy over distance to go is partitioned into five membership functions, which are shown in Fig. 7a.

In this work, we assume that control surface health is being monitored by a separate subsystem. For convenience, the control surface health signal is simulated by four possible integer values that correspond to four values of maximum bank angle. Degraded control surfaces were simulated simply by limiting the maximum bank angle. Considering computation of X_{HAC} to be a two-input fuzzy inference with five-input membership functions on the first input (E_W/R_{ALI}) and four-input membership functions on the second input (control surface health) results in 20 possible combinations for which we provide 20 total rules. The rules for X_{HAC} determination are shown

Table 2 Rules for determining X_{HAC} from inputs E_W/R_{ALI} and degree of control degradation

Degree of control degradation	E_{MEP}	E_N	SS	SM	SL
Zero	X_{MEP}	X_{ALI}	X_{FTC}	X_{FTC}	X_{max}
Slight	X_{ALI}	X_{ALI}	X_{max}	X_{max}	X_{max}
Moderate	X_{ALI}	X_{ALI}	X_{FTC}	X_{FTC}	X_{max}
Severe	X_{ALI}	X_{ALI}	X_{MEP}	X_{FTC}	X_{FTC}

Table 3 Default HAC turn radii

Aero failure	Maximum bank, deg	HAC radius, ft
Zero	56	26,000
Slight	46	33,000
Moderate	36	41,000
Severe	26	50,000

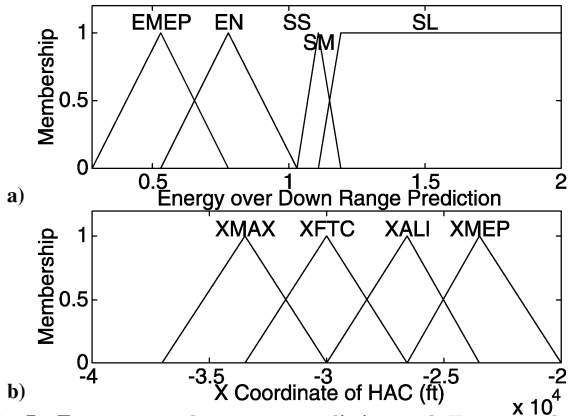

Fig. 7 Energy over downrange prediction and X_{HAC} membership functions.

in Table 2, where the degree of control surface degradation partitions are shown as row headings and the partitions of E_W/R_{ALI} are shown as column headings. The associated output membership functions for the 20 rules are shown in the body of Table 2. The partitioning of the output universe of discourse for X_{HAC} is shown in Fig. 7b.

Projectiles in ballistic flight typically have an airspeed profile that is an exponential decay with respect to downrange distance. In the current work, several nominal gliding trajectories were examined, and a profile that is linear with respect to ground distance was chosen as adequate. This profile, shown in Eq. (22), is used to predict the velocity at HAC intercept. The lower limit of 820.97 ft/s is based on the dynamic pressure limit for stall at nominal HAC intercept altitude:

$$V_{HAC} = \max \begin{cases} V - R_1 0.0326 \\ 820.97 \end{cases} \tag{22}$$

where R_1 is the distance to HAC intercept in feet. The expected turn radius for the HAC turn r_{HAC} can be computed from the expected velocity at HAC intercept V_{HAC} and maximum bank ϕ_{max}:

$$r_{HAC} = V_{HAC}^2 \Big/ g \tan \phi_{max} \tag{23}$$

The HAC turn radius is set to the minimum of expected radius and value from Table 3. Center-of-gravity defuzzification is used in all fuzzy decisions in this paper. A second fuzzy inference system determines the maximum bank angle allowed, ϕ_{max}, based on the state of control surface health.

Bank Guidance Commands

The bank guidance commands are generated by a fuzzy inference system with 7 inputs, 112 rules, and a single output. The inputs are 1) TAEM subphase, 2) ratio of actual turn radius to desired HAC radius, 3) degrees of turn to HAC center, 4) perpendicular distance from extended runway centerline, y, 5) runway y-axis component of velocity, $\dot{y}$, 6) a flag denoting HAC turn direction, and 7) relative bearing from the aircraft x axis to the center of the HAC turn. The conventional subphases of TAEM, which are acquisition, HAC turn, and prefinal,[12] are used to limit the number of inputs that must be considered during a single iteration. For each subphase of TAEM, the system uses the relevant inputs to determine an appropriate bank angle. During the acquisition turn, the only input considered is turn angle to the HAC center, $\Delta\Psi_{aq}$, which is partitioned into five membership functions. In this phase, the fuzzy inference system acts as a proportional controller with five rules connected to the five-output membership functions. That is, a large difference in heading angle from HAC center will produce a large bank angle in the appropriate direction. Likewise, as the difference in heading angle decreases to $\frac{1}{2}$ deg, the guidance commands the spacecraft to roll out gradually. The acquisition turn ends when the spacecraft is pointed within $\frac{1}{2}$ deg of the HAC center, or when it reaches a range of 1.85 HAC radii from the HAC center, to facilitate intercepting the HAC arc.

The basic rules for bank guidance during HAC turn are taken from techniques taught to military instrument pilots. The baseline geometry of the trajectory follows a typical TACAN approach, where the aircraft is flown directly toward the TACAN, intercepts a circular arc around the TACAN, then completes a base turn to final approach. The discussion that follows further illustrates the use of instrument flying techniques in designing the fuzzy inference system for bank commands.

To fly a constant radius turn around a TACAN, the pilot turns the aircraft to position the TACAN on the wing. To maintain a constant radius, the pilot must consider both the distance from the TACAN and relative bearing. Thus, during the HAC turn, the relevant inputs are turn radius error, bearing to the HAC center, and turn direction. Bearing to the HAC center is divided into 13 membership functions with fine divisions near the wing where precise control is required. Turn radius error is expressed as a ratio of current turn radius over desired turn radius and is partitioned into seven membership functions. These partitions are shown in Fig. 8. During this phase, 89 rules are used.

The rules corresponding to right turns are shown in Table 4, where the first column is bearing and the first row is turn radius error.

Table 4 Bank rules for right turns around HAC from inputs turn radius error and bearing to HAC center

Bearing to HAC center	LP	MP	SP	Z	SN	MN	LN
Nose	Z	N	LN	LN	LN	LN	LN
RF45	Z	Z	N	LN	LN	LN	LN
RF10	LP	LP	P	Z	N	LN	LN
Rwing	LP	LP	P	P	Z	N	LN
RA10	LP	LP	LP	LP	Z	Z	N
RA45	LP	LP	LP	LP	P	Z	Z
Tail	LP	LP	LP	LP	LP	LP	LP

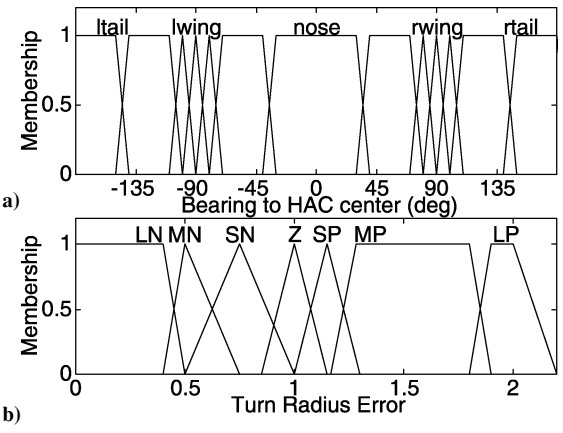

Fig. 8 Partitioning of station bearing and turn radius error inputs.

Bearing uses the abbreviations nose to denote the quadrant forward of the spacecraft, RF45 to denote the right forward quadrant, RF10 to mean approximately 10 deg forward of the right wing, wing, etc. Some rules do not consider turn direction, such as when approaching the HAC from far away. These rules are based on the author's own flight experience totaling more than 2000 h in military jet aircraft and relevant portions of Ref. 12. In the most basic sense, the rules for tracking the desired HAC radius can be seen as position and rate error feedback. That is, relative bearing provides an approximation of turn radius rate error. An aircraft that is approaching the HAC turn with HAC center nearly aligned with the aircraft nose will have a positive turn radius error, but this error is decreasing rapidly. Thus, the appropriate action is to turn away from the HAC center. Turn direction is determined by a flag based on the sign of initial runway y coordinate because only a direct or straight-in approach is used in this work. The rules for HAC subphase cause the spacecraft to execute an approximately 90-deg turn to intercept the HAC, then correct perturbations from the desired HAC radius until reaching prefinal transition. Prefinal transition is triggered when the spacecraft heading is within 45 deg of runway heading and perpendicular distance from extended runway centerline is decreasing.

During prefinal phase, the control objective is to position the aircraft on extended runway centerline, aligned with runway heading. Thus, the relevant inputs are the components of aircraft position and velocity perpendicular to runway centerline. We use 14 rules to guide the aircraft aggressively back to runway. According to Eq. (17), velocity perpendicular to runway centerline is directly related to heading angle. When the geometry is drawn for all combinations of runway y coordinates and heading angles represented by the input membership functions, the rules for this phase can be written from intuition gained by driving a car or flying an airplane. For instance, if y is P, but the spacecraft heading causes $\dot{y}$ to be LN, the appropriate action is an aggressive turn to the right or bank is LP. TAEM guidance ends when the altitude, runway Y coordinate, flight-path angle, and dynamic pressure are all within approach and landing transition tolerances, or the spacecraft reaches a minimum altitude for approach and landing transition.

Note that the bank fuzzy inference system provides the proportion of available bank to be used as shown by the output membership functions in Fig. 4. The maximum available bank angle is determined as part of the acquisition turn trajectory planning. Maximum bank nominal values are shown in the middle column of Table 3. Bank guidance is computed as the product of maximum bank and the output of the bank fuzzy inference system The bank commands are then smoothed by a first-order unity gain low-pass filter with cutoff frequency of 0.5 rad/s before transmission to the flight control system. This smoothing alleviates controller saturation and subsequent instability during abrupt changes in guidance caused by TAEM subphase changes.

Negative z-Axis Acceleration Guidance

The negative z-axis acceleration guidance commands are determined by a fuzzy inference system with four inputs and 52 rules. The inputs are altitude error, vertical velocity error, dynamic pressure, and Mach number. The altitude error and vertical velocity error inputs are divided into five membership functions each. Thus, there are 25 rules for $\bar{q}$ in the medium range, which are replicated for both subsonic and supersonic flight. These basic rules act as a proportional–derivative controller to align the spacecraft with the desired glidepath. As in the earlier guidance rule sets, the rules for negative z-axis acceleration are based on the desired action for tracking a path given position and rate error. In this case, the path is an incline in the vertical plane. The 25 basic rules are shown in Table 1 where the first column is the vertical velocity error and the first row is the altitude error.

The membership function partitions for altitude error and vertical velocity error are shown in Fig. 3. The membership function partitions for bank angle and normal acceleration output commands are shown in Fig. 4. Note that the negative z-axis acceleration guidance commands are limited to $\pm 0.6\ g$ to ensure that the lift capability of the spacecraft is not exceeded.

The X-33 has no physical speed brake. The inner-loop flight control system reacts to speed brake commands by an asymmetric positioning of the body flap and elevons. During supersonic flight, this asymmetric component is limited to zero, and dynamic pressure is controlled by pitch attitude alone. During subsonic flight, no thrust is available; therefore pitch alone must be adjusted to avoid a stall condition. Thus, the following two rules are employed to keep the dynamic pressure within nominal limits for supersonic flight and above the stall limit for subsonic flight:

1) If $\bar{q}$ is low, then N_Z is large negative.
2) If $\bar{q}$ is high and $M > 1$, then N_Z is positive.

Results

The described fuzzy inference systems were rapidly prototyped, tuned, and tested using MATLAB and the fuzzy logic toolbox. The simplified three-degree-of-freedom dynamics described earlier were programmed in MATLAB and served as an adequate model of a reusable launch vehicle in the TAEM phase. The described fuzzy inference systems were developed by formalizing a combination of the author's own personal knowledge of instrument flying and the expertise found in the existing shuttle TAEM guidance. Extensive trial and error followed until the fuzzy algorithms could control the simplified dynamics to a satisfactory level. In particular, partitioning of the input space for each channel was done through careful observation of the state variables (altitude, forward velocity, vertical velocity, etc.) during high-fidelity simulations with existing shuttle TAEM guidance. That is, the terms large positive, medium negative, etc., were associated with numerical values by observing how much each input and output variable changes under existing guidance algorithms.

The X-33 was a suborbital, single-stage, autonomous, reusable launch vehicle. It was intended to demonstrate the technologies needed to develop the VentureStar, which was intended to be a full-scale replacement for the shuttle. Although the X-33 program has been canceled, the high-fidelity models and simulations that were built as part of the program are unique in their maturity and utility. X-33 is currently the only vehicle that can be simulated in all phases of flight on the Marshall Aerospace Vehicle representation in C (MAVERiC)[13,14] simulation package. After obtaining satisfactory results that demonstrated robustness to varying initial conditions and degrees of control surface health, the fuzzy systems were integrated with the high-fidelity six-degree-of-freedom simulation known as MAVERiC. Limited further tuning was required to replicate the results obtained in MATLAB. Because the initial design and tuning only requires a rough model, the same guidance laws should be readily adaptable to the next-generation reusable launch vehicle.

The ground track and bank angle of four high-fidelity simulations are shown in Fig. 9. The solid lines represent the trajectory with full flight control authority. Dotted lines represent the trajectory when flight controls are degraded such that bank angle is limited to 36 deg. The axes on the ground track plot do not have equal scaling, allowing differences to be emphasized. The four cases shown represent the limits on initial heading to reach a successful landing. Varying the heading by ± 30 deg creates an energy initial state lower than nominal because maneuverability is limited at TAEM initiation and

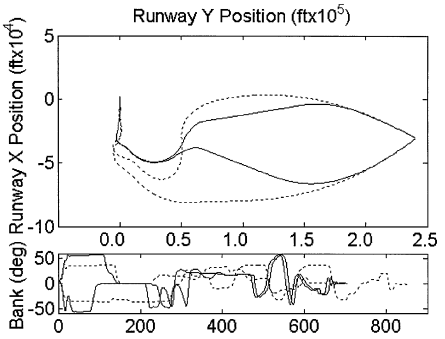

Fig. 9 Vehicle ground track and bank angle for various initial headings and bank restrictions.

Table 5 Initial conditions tested and ALI envelope demonstrated

Variable and unit	Initial condition range tested	Range observed at ALI
Range to runway, ft	$216{,}000 < R < 280{,}330$	$10{,}101 < R < 12{,}967$
h, ft	$78{,}000 < h < 88{,}500$	$4784 < h < 4881$
Mach	3.02	$0.469 < \text{Mach} < 0.481$
$\dot{h}$, ft/s	-270	$-449 < \dot{h} < -214$
ψ, deg	$236 < \psi < 297$	$356.6 < \psi < 5.6$
γ, deg	-6.16	$-24.4 < \gamma < -28.8$

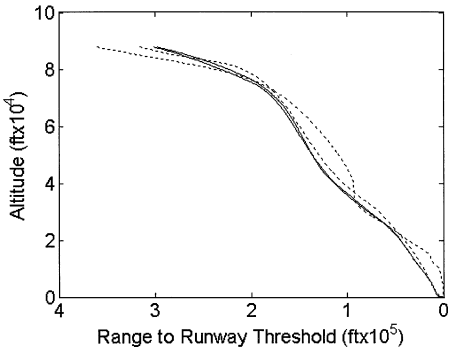

Fig. 10 Vehicle altitude for various initial headings and bank restrictions.

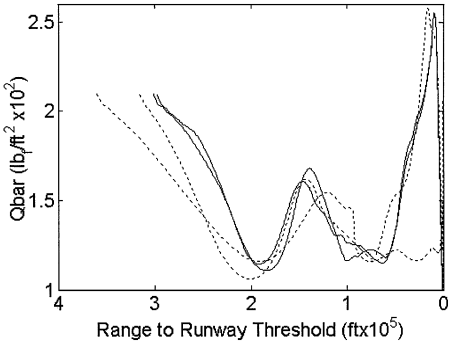

Fig. 11 Dynamic pressure for various initial headings and bank restrictions.

the vehicle must fly a significantly longer ground track to turn back. The actual maximum bank used during degraded flight is 38.44 deg. All four cases plotted reach a successful landing at 1500–2500 ft from the runway threshold and within 33.64 ft of runway centerline.

At least 12 additional cases were run to test the limits on initial range from runway and altitude, as well as to repeat the initial heading range test for various degrees of maneuver restriction. The initial conditions tested are given in Table 5. The initial and final heading angle are shown as a compass heading with respect to runway heading. Thus, the range observed at ALI is actually from 3.4-deg left of runway heading to 5.6-deg right of runway heading. The envelope for successful ALI is defined by the maximum possible perturbation that existing shuttle autoland guidance can tolerate at ALI and still reach a successful landing. This envelope observed throughout all testing is shown in Table 5.

Figure 10 shows the corresponding altitude profiles for the four simulations of Fig. 9. Both full control cases and one of the degraded cases converge to the desired ALI conditions. The degraded case with initial heading farthest to the right reaches ALI very steep and high.

The corresponding dynamic pressure profiles are shown in Fig. 11. Note that all trajectories stay within the nominal limits of 100–300 lbf/ft^2.

Additional tests were run to vary the initial distance from ALI and the initial altitude. The minimum altitude at TAEM interface for successful landing was found to be 78,000 ft. The maximum altitude was found to be 88,500 ft. This does not represent an improvement over current guidance.

One fascinating discovery is that the fuzzy inference systems have complementary effects on each other although each channel was designed separately. For example, for a case with flight control limitations and nominal initial energy, the trajectory designer will direct a wide radius HAC. The ground track predictor then computes a longer than normal ground track. Subsequently, the normal acceleration guidance keeps the flight-path angle shallow during the acquisition phase of flight. The shallower glide path is then advantageous to the bank guidance because the spacecraft will reach subsonic flight sooner and will, thus, be ready to intercept the HAC.

Conclusions

Fuzzy logic control is extremely powerful for control of complex systems without precise models. Several fuzzy inference systems have been designed by application of the knowledge base from shuttle TAEM guidance and the author's own flight experience. These fuzzy systems were tuned by trial and error on a very simple set of dynamics then programmed into a high-fidelity six-degree-of-freedom simulation. Although each channel of the fuzzy guidance system was designed separately and tuned on dynamics where the axes were completely decoupled, the new guidance system still performed well on the high-fidelity simulation where the dynamics are very realistic. In fact, the separate channels show complimentary effects. The fuzzy logic approach also provides true autonomous trajectory design, where the trajectory parameters may take any value from within a specified range. Fuzzy logic provides a straightforward way of dealing with multiple conflicting objectives, such as a large energy dispersion accompanied by control surface degradation. The high-fidelity simulations demonstrate an ability to design and fly gliding return trajectories autonomously for varying initial energy conditions and stringent maneuver restrictions.

Acknowledgments

This work was supported by NASA Contract NAG81786. The author is greatly indebted to J. Hanson of the NASA Marshall Space Flight Center for providing both the intellectual and financial impetus for this research. A great deal of assistance was received from G. Dukeman and J. McCarter of NASA Marshall Space Flight Center regarding intricacies of the MAVERiC high-fidelity simulation.

References

[1]Barton, G. H., and Tragesser, S. G., "Autolanding Trajectory Design for the X-34," AIAA Paper 99-4161, 1999.

[2]Barton, G. H., "New Methodologies for Assessing the Robustness of the X-34 Autolanding Trajectories," *Advances in the Astronautical Sciences*, Vol. 107, *Guidance and Control*, 2001, pp. 193–214.

[3]Girerd, A., and Barton, G., "Next Generation Entry Guidance–Onboard Trajectory Generation for Unpowered Drop Tests," AIAA Paper 2000-3960, Aug. 2000.

[4]Grantham, K., "Adaptive Critic Neural Network Based Terminal Area Energy Management/Entry Guidance," AIAA Paper 2003-0305, Jan. 2003.

[5]Hanson, J. M., "New Guidance for New Launchers," *Aerospace America*, Vol. 41, No. 3, 2003, pp. 36–41.

[6]Vinh, N. X., *Optimal Trajectories in Atmospheric Flight*, Elsevier, New York, 1981, Chap. 3.

[7]Von Mises, R., *Theory of Flight*, Dover, New York, 1959, pp. 9, 10.

[8]Lee, C. C., "Fuzzy Logic in Control Systems: Fuzzy Logic Controller—Part I," *IEEE Transactions on Systems, Man, and Cybernetics*, Vol. 20, No. 2, 1990, pp. 404–417.

[9]Jamshidi, M., dos Santos Coelho, L., Krohling, R., and Fleming, P., *Genetic Algorithms in Robust Control*, CRC Press, Boca Raton, FL, 2003, p. 199.

[10]Larkin, L. I., "A Fuzzy Logic Controller for Aircraft Flight Control," *Industrial Applications of Fuzzy Control*, edited by M. Sugeno, Elsevier Science, North-Holland, Amsterdam, 1985, pp. 87–103.

[11]Moore, T. E., "Space Shuttle Terminal Area Energy Management," NASA TM 104744, Nov. 1991.

[12]*Instrument Flight Procedures*, U.S. Air Force Manual 11-217, Vol. 1, 29 Dec. 2000, URL: http://afpubs.hq.af.mil.

[13]McCarter, J., *Maveric Users Guide*, NASA/MSFC/TD54, June 1999.

[14]Hanson, J., Coughlin, D., Dukeman, G., Mulqueen, J., and McCarter, J., "Ascent, Transition, Entry, and Abort Guidance Algorithm Design for the X-33 Vehicle," AIAA Paper 98-4409, Aug. 1998.

C. A. Kluever
Associate Editor